Identification of the 9-Aminoacridine/DNA Complex Responsible for Photodynamic Inactivation of P22†

Edward L. Loechler* and Jonathan King

Department of Biology, Massachusetts Institute of Technology, Cambridge, Massachusetts 02139

Received July 22, 1985; Revised Manuscript Received May 5, 1986

ABSTRACT: Acridine dyes bound to the condensed DNA within phage particles sensitize them to inactivation by visible light. The mechanism involves absorption of photons by an acridine/DNA complex, generating singlet oxygen, which covalently damages nearby proteins needed for DNA injection [Bryant, J., & King, J. (1985) *J. Mol. Biol. 180*, 837–863]. Acridines and related dyes interact with double-stranded DNA through a number of binding modes. To determine in condensed phage DNA the binding mode responsible for this inactivation, we have studied the formation of the DNA/acridine target complexes for photoinactivation. Analysis of the kinetics of 9-aminoacridine binding to *Salmonella* phage P22 particles revealed the formation of two binding species, one of which appeared more rapidly and was apparently an intermediate in the formation of the second. The rapidly forming species represented DNA sites with intercalated acridines, while the more slowly forming species represented the subsequent binding of additional acridine molecules to the DNA backbone of sites already containing intercalated dye. The rates of photoinactivation correlated with the rate of binding of 9-aminoacridine to the DNA backbone. This suggests that the most effective species for sensitizing phage to light-induced damage has acridine molecules stacked alongside the backbone of a region with intercalated molecules.

The resting state of double-stranded DNA in the genomes of most organisms is highly condensed with respect to the state of DNA free in solution. The interactions of such condensed DNA sites with mutagens and carcinogens are likely to be different from the solution states. We have studied the interaction of acridine dyes with the chromosomes of bacterial viruses which are about 250-fold condensed within the mature particle (Earnshaw & Casjens, 1980). In the presence of acridines and related dyes, many bacterial viruses are inactivated upon exposure to visible light. This process, referred to as photodynamic inactivation, provides a probe for the formation of specific acridine/DNA target complexes.

Photodynamic treatment inactivates many viruses and kills many microorganisms (Welsh & Adams, 1954; Yamamoto, 1958; McLaren & Shuger, 1964; Alberts, 1966; Spikes, 1977; Calberg-Bacq et al., 1977a,b). This inactivation is known to require a photodynamically active dye, light, and molecular oxygen (Foote, 1968). Steps in the mechanism(s) of viral inactivation include the binding of the dye at some critical site, the photoexcitation of this dye molecule, and the subsequent production of a reactive intermediate, which damages a crucial, viral macromolecule and thus renders the virus nonviable.

Most of the photodynamically active dyes, such as the acridines, form noncovalent complexes with DNA (Lerman, 1961, 1963; Peacocke, 1973). Two classes of binding sites are known. One type involves strong binding (process I) and is associated with dye intercalation between the stacked bases of DNA (Blake, 1968; Peacocke, 1973). The structures of the intercalated forms of 9-aminoacridine (9aa) and several other dyes have been determined by X-ray diffraction (Sakore et al., 1977; Tsai et al., 1977; Jain et al., 1977; Sobell et al., 1977; Neidle et al., 1977). A second type of interaction involves weaker binding (process II) and is associated with the binding of the positively charged dye to the phosphates of the DNA backbone (Weill & Calvin, 1963; Schwarz & Sigmar, 1972; Dourlent & Hogrel, 1976; Yamaoka & Masujima, 1978). A structure for this binding mode with methylene blue has been proposed on the basis of linear and circular dichroism spectroscopy (Norden & Tjerneld, 1982).

Two photodynamic processes have been described that produce reactive, potentially damaging species (Piette et al., 1977, 1981a,b). The type I mechanism is biphotonic and produces radicals in the DNA bases which ultimately gives rise to peroxide radicals (formed from dissolved molecular oxygen) in DNA (Van de Vorst & Lion, 1971, 1973). The type II mechanism is monophotonic and produces highly reactive singlet oxygen from ground-state triplet oxygen (Foote, 1968; Spikes & Livingston, 1969; Lochman & Micheler, 1973).

To investigate these phenomena, we have utilized the well-characterized *Salmonella* bacteriophage P22. The structure of the DNA within P22 has been studied by low-angle X-ray scattering (Earnshaw & Harrison, 1977). The strands are locally close-packed and parallel, organized overall in concentric coils, probably around a unique axis, like a spool of rope (Earnshaw et al., 1976). The coiled DNA of P22 is contained in a simple protein shell composed primarily of a single major coat protein (gp5) along with seven other minor proteins, which form the DNA injection and cell attachment organelle (King et al., 1976; Murialdo & Becker, 1978).

P22 is rapidly inactivated by a variety of photodynamically active agents, including the acridines. Bryant and King (1985) found that damage to the DNA injection proteins (gp7, gp16, and gp20) of the P22 particle was the event responsible for the inactivation. This damage does not occur in P22 particles lacking DNA, which suggests that a protein/DNA/9aa complex is necessary for inactivation. In this paper, we present evidence to show that the binding site crucial to inactivation has 9aa bound to the DNA backbone.

† This work was supported by NIH Grant GM17980 to J.K., by NIEHS Grant IP30-ES021-09-01 to Gerald Wogen, and by an NIEHS Fellowship to E.L.L.

* Address correspondence to this author at the Department of Biology, Boston University, Boston, MA 02215.

0006-2960/86/0425-5858$01.50/0

Materials and Methods

The bacterial strain used in this study was a derivative of *Salmonella typhimurium* LT2 from the collection of Dr. David Botstein, DB 7004 (Su^+) (Susskind et al., 1974). Unless otherwise specified, all the P22 strains contained the c*1*-7 clear plaque allele to prevent lysogeny and the *13*⁻ amH101 allele to delay lysis. Bacteria and phage were grown as described in Botstein et al. (1973) and Earnshaw and King (1978). The titer of infectious phage was determined by the standard soft agar plaque assay (Adams, 1959).

Chemicals and Buffers. Stock solutions of 9-aminoacridine hydrochloride (Eastman Kodak, laser grade) were made up in double-distilled water and stored at 4 °C in the dark. All other salts and buffers were reagent grade. All inactivation and binding experiments were carried out in 7.5 mM tris(hydroxymethyl)aminomethane hydrochloride (Tris·HCl)/3.75 mM $MgCl_2$, pH 7.4.

Phage Inactivation. A plant growth lamp (General Electric, 150 W), which has a low UV output, was used as the light source in the inactivation experiments. The phage solutions were illuminated in 11-mm Pyrex test tubes (50% transmittance at 286 nm) for the times indicated in the text or figure legends. The tubes were 15 cm from the light source unless otherwise noted. The fluence was determined to be 230 and 1150 J/m²·s in the range of 400–1000 and 300–30 000 nm, respectively, when measured at 15 cm.

In the kinetic experiments, the light-induced inactivations were halted by removing aliquots from the reaction tubes, diluting the sample by 100-fold, and quickly shielding the resulting mixture from the light.

Light intensity was varied by changing the distances between the light source and the sample. Intensity was assumed to vary as the square of the distance. The experiments, which involved varying the light intensity, were performed to determine if the inactivation was mono- or biphotonic. Biphotonic reactions require photons of different energies (Van de Vost & Lion, 1971, 1973). With white light, as the distance between the light source and sample was varied, the intensity of photons at both energies would be decreased. Thus, the rate of a biphotonic reaction would vary according to the square of the light intensity.

Anaerobic conditions were established by a slight modification of the procedure used by Loechler and Hollocher (1980).

Inactivation Kinetics. Observed pseudo-first-order rate constants were determined from the slope of the linear portions of plots of the log of surviving P22 vs. time, according to

$$k_{obsd}\ (\text{min}^{-1}) = \text{slope ln } 10$$

In experiments where P22 and 9aa were incubated together in the dark prior to illumination, the inactivation was approximately linear throughout the inactivation. Upon occasion, the data appeared to show a brief lag, which was ignored.

Binding Curves and Optical Density (OD) Determination. Absorbance measurements were determined on a Beckman DU monochromator modified with a Guilford detector. All OD values are ±0.002 ODU, and ΔOD are ±0.004 ODU.

To determine the total change in OD (measured at 400 nm) that occurs upon adding P22 particles to solutions of 9aa, the following protocol was carried out. 9aa was mixed with P22, and the change in OD was followed for 1 min. From these data, an OD_0 value was determined by plotting log ($OD - OD_\infty$) vs. time and back-extrapolating to the OD value at zero time. This value is very accurate, because the first time point was usually taken at $t = 10$ s. After following the OD change for 1 min, the cuvette was removed from the spectrophotometer and stored in the dark for 60 min. At that time, the cuvette was placed back into the spectrophotometer, and the OD ($=OD_\infty$) was recorded. The change in OD was determined according to $\Delta OD = OD_0 - OD_\infty$. This procedure ensured that the OD value was determined in the dark and thus the effect of light on binding was eliminated (see Discussion).

One potential complication can arise from the fact that at high concentrations of 9aa, 9aa self-association occurs. To minimize this potential complication, experiments were performed at 9aa concentrations no greater than 100 μg/mL. On the basis of spectrophotometric work, our estimate of the 9aa self-association constant is $K = 140 \pm 70\ M^{-1}$. Thus, at 100 μg/mL, 10% of the 9aa would be aggregated into a dimer. Under somewhat different conditions, Young and Kellenback (1981) estimated $K = 265 \pm 90\ M^{-1}$ for 9aa self-association.

Results

In the presence of a variety of aromatic, heterocyclic compounds, P22 particles were inactivated upon irradiation with visible light (Bryant & King, 1985). As described under Materials and Methods, pseudo-first-order rate constants of inactivation were determined from the slopes of straight lines drawn through data plotted as the log of viable P22 vs. time of incubation in the light (data not shown). The inactivation had the characteristics of a photodynamic process in that it did not occur in the absence of light, 9aa, or oxygen.

In order to characterize the target within the P22 particle where 9aa must bind before inactivation can occur, we have carried out a detailed analysis of (i) the kinetics of binding of 9aa to P22 and (ii) the kinetics of inactivation.

9aa Binding to P22 Particles. The absorption spectrum of 9aa showed a marked hypochromicity upon the addition of P22 particles (data not shown). Under comparable conditions, phage capsids lacking DNA showed less than 10% of this hypochromicity (data not shown). Thus, this effect appears to be due to 9aa interactions with DNA within the phage head. Others have made similar observations in related systems and have reached the same conclusion (Sharp & Bloomfield, 1970).

Figure 1 (closed circles) shows the effect of 9aa concentration on the magnitude of the decrease in absorbance that was observed at 400 nm when P22 particles were added to a solution of 9aa. At lower [9aa], a small change in OD is observed, which probably reflects a tight binding process (I). At higher [9aa], a second, weaker binding process (II) is observed. The sigmoidal appearance of this portion of the binding curve probably reflects positive cooperativity in the binding of 9aa to P22 (see Discussion).

Phage/9aa mixtures, under conditions identical with those used in the experiments described above, were also irradiated with white light to measure the rates of inactivation. The open circles in Figure 1 show the effect of [9aa] on the observed rate constants of inactivation, and a smooth curve is drawn through the data.

Kinetics of 9aa Binding to P22 Particles. When P22 particles were added to a solution of 9aa, the absorbance gradually decreased with time as 9aa molecules became bound to the DNA of the P22 particle. Figure 2 shows a typical time course of 9aa binding to P22; a triphasic curve is observed. For ease of explanation, we will ignore for the moment the third phase of this curve, which is observed at times greater than 10 min. The data at times less than 10 min can be fit according to

$$OD - OD_\infty = Ae^{-k_X t} + Be^{-k_Y t}$$

where the $e^{-k_Y t}$ term represents the slower, second phase, which dominates between 2 and 10 min. When this slower phase is

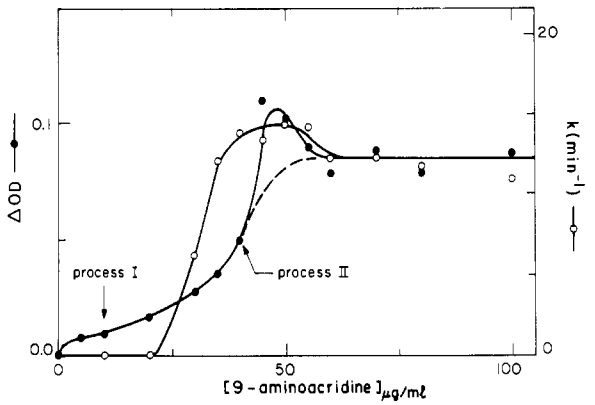

FIGURE 1: Relationship between the amount of 9aa bound to P22 particles and the rate constants of inactivation. The difference in the absorbance of a 9aa solution in the presence and the absence of 10^{10} viable P22 particles at 400 nm after 60-min preincubation in the dark (ΔOD) is plotted vs. 9aa concentration in micrograms per milliliter. These data (closed circles) use the scale on the left-hand ordinate and are connected by a smooth curve. The open circles (right-hand ordinate) show the rate constants of inactivation under the same conditions, also after 60-min preincubation in the dark. The hump observed at [9aa] = 50 μg/mL is reproducible, and its origin is not understood.

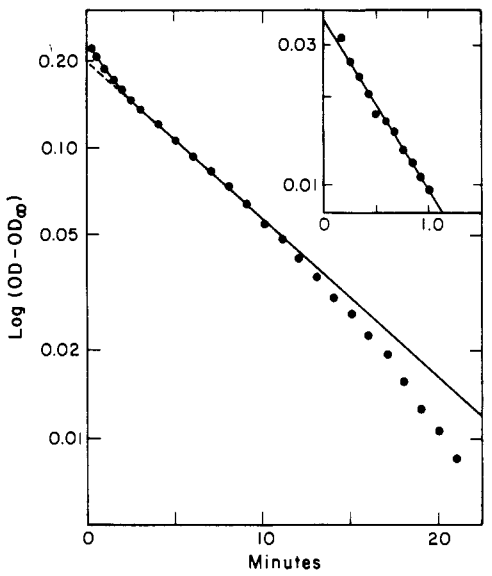

FIGURE 2: Kinetics of binding of 9aa to P22 particles. A total of 10^{10} viable P22 particles [The discrepancy between total ΔOD when comparing Figures 1 and 2 results from the fact that different P22 phage stocks were used, and the ratio of viable to nonviable phage typically varies between stocks (J. King, unpublished observation). More particles (total) were used in the experiment in Figure 2, so that positive cooperativity could be demonstrated more convincingly.] was added to a 9aa solution (100 μg/mL), and the absorbance at 400 nm was monitored. The OD decreased with time and eventually reached a plateau (the OD value at the plateau is designated OD_∞). The log of the OD at any time minus OD_∞ is plotted vs. time (closed circles). The data at times less than 10 min can be fitted by an equation in the text which was derived for a two-step, sequential binding reaction. The slower rate constant (k_Y) can be estimated by drawing a straight line through the data (closed circles) at times between 2 and 10 min. By use of this estimate of k_Y, the faster rate constant (k_X) can be determined; a plot of the data treated in this way is shown in the insert. k_X = 1.3 min^{-1} and k_Y = 0.12 min^{-1}. The increase in rate at times greater than 10 min has been attributed to positive cooperativity in the second binding step (k_Y).

subtracted from the data, the more rapid, initial phase of the reaction is isolated (Figure 2, insert). This phase is associated with the $e^{-k_X t}$ term.

The two-phase, kinetic reaction seen in Figure 2, prior to 10 min, is consistent with Scheme I, where X and Y represent

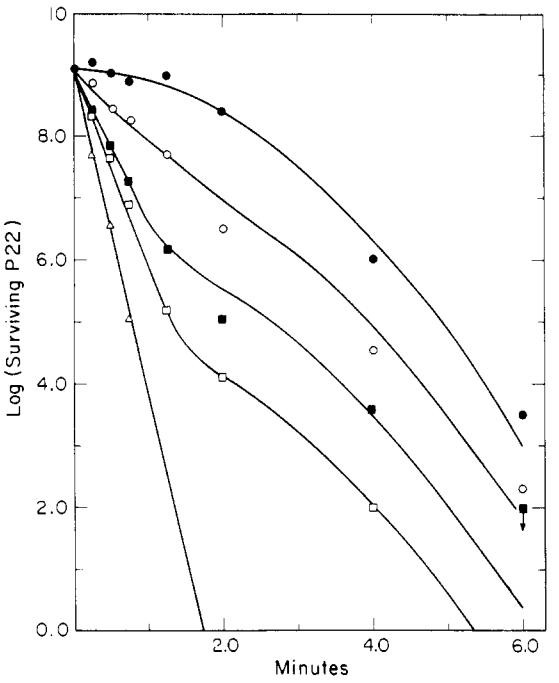

FIGURE 3: Change in the inactivation curves as a function of the time that P22 and 9aa (=100 μg/mL) were preincubated together in the dark. The data are plotted as the log of surviving P22 vs. time of exposure to light. Prior to light exposure, P22 was preincubated in the dark with 9aa for 0 (●), 2.5 (○), 5.0 (■), 7.5 (□), and 24 min (△). Incubation curves were also done at 10 and 12.5 min of dark preincubation as well, but for clarity these have not been included in this figure.

two species that have 9aa bound to the DNA of P22. Scheme I would be adequate to describe the data in Figure 2, if all X- and Y-type binding sites behaved equivalently. However, we see evidence that positive cooperativity is observed in binding (Figure 1). Positive cooperativity is observed in the kinetics as well. In Figure 2 it manifests itself as the increase in rate at longer time, i.e., as the third phase at times greater than 10 min. Because of this apparent cooperativity, Scheme I is not adequate to describe the data. However, we find that it is a useful approximation (especially at shorter times) and it facilitates the analysis of much of the data.

Scheme I

$$\text{P22} + \text{9aa} \xrightarrow{k_X} \text{X} \xrightarrow{k_Y} \text{Y}$$

Kinetics of the Diffusion of 9aa to the Site Responsible for Inactivation. To further investigate the 9aa binding site within P22 responsible for inactivation, a study of the changes in the rate constants of inactivation as a function of preincubation time in the dark was carried out. The protocol was as follows: (1) at time zero, P22 was mixed with 9aa in the dark; (2) following preincubation in the dark for various times, samples were removed and put into the light; (3) aliquots were removed from these samples at varying times in the light; and (4) the level of P22 survival was subsequently determined. Thus, a series of inactivation curves were generated, which varied only in their time of preincubation in the dark.

Figure 3 shows the results of such an experiment. As the dark preincubation time increases, the rate of the inactivation reaction also increases. This indicates that during the dark preincubation period, 9aa is diffusing to its crucial target site and that the inactivation rate from this target is faster than the diffusion of 9aa to the target. Thus, the changes in these curves with preincubation time reflect the rate at which 9aa gets to the crucial target which must be occupied before in-

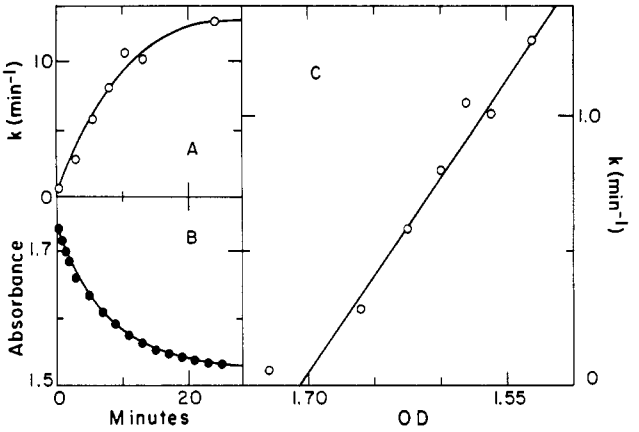

FIGURE 4: Relationship between the kinetics of 9aa binding to P22 particles and the kinetics of the inactivation reaction. (A) Plot of the initial rate of the P22 inactivation process (data from Figure 3) as a function of the time that P22 and 9aa (=100 μg/mL) were preincubated together in the dark. (B) Plot of the observed absorbance decrease as a function of time after P22 particles were added to a 9aa (=100 μg/mL) solution (data from Figure 2). (C) Plot of the inactivation rate constants (from panel A) vs. OD (from panel B). At each time point for which there was an inactivation rate constant, a corresponding OD from the binding curve was interpolated. A straight line was drawn through the data.

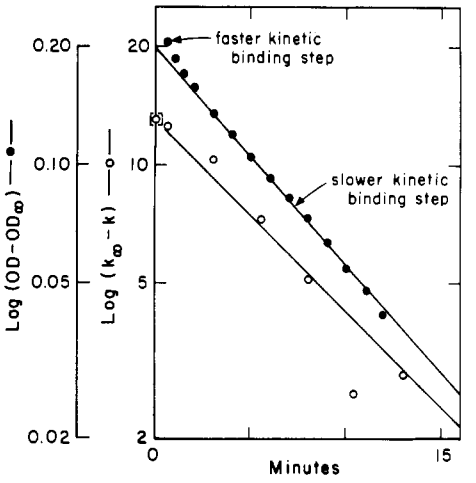

FIGURE 5: Semilog plot of the data from Figure 4A,B. k_∞ was determined as described under Materials and Methods, and log ($k_\infty - k$) is plotted against time [(○) data from Figure 4A]. A straight line was drawn through the data. This plot gives $k_3 = 0.11$ min^{-1}. Likewise, OD_∞ was determined, and log ($OD - OD_\infty$) is plotted against time [(●) data from Figures 2 and 4B]. A straight line was drawn through the time points after the initial faster reaction ($k_Y = 0.12$ min^{-1}).

activation can occur. Only the initial rate data (the first several minutes in Figure 3) will be discussed under Results. A straight line was drawn through these initial points and the rate constants determined.

Figure 4A shows the change in these rate constants of inactivation (determined from the data in Figure 3) as a function of the dark preincubation time. They increase and approach a limit. In Figure 4B, a kinetic binding curve determined under similar conditions is shown as a plot of OD vs. time. A comparison of these figures reveals a correlation between the amount of 9aa bound at any time (Figure 4B) and the magnitude of the rate constant of inactivation (Figure 4A) at the same time. This correlation can be seen more clearly in Figure 4C, which shows a plot of the data in Figure 4A vs. that in Figure 4B; a linear relationship is observed between the initial rate constants of inactivation and the change in OD.

Figure 5 shows a semilog plot of the data from Figure 4A,B, i.e., a plot of both log ($k_\infty - k$) and log ($OD - OD_\infty$) vs. time. The curves are nearly parallel, which suggests that they are related. In fact, it is the slower of the two kinetic binding steps, associated with the formation of Y by k_Y in Scheme I, which correlates with the change in the rate constants of inactivation. These results imply that the target complex for 9aa photodynamic inactivation is species Y in Scheme I.

Dependence of the Inactivation Rate Constant on the Intensity of Light. Dye-sensitized photodynamic inactivation processes requiring either one or two photons (type II and type I mechanisms, respectively) have been reported (Van de Vorst & Lion, 1971, 1973; Piette et al., 1977, 1981a,b). We investigated which applied for P22 inactivation. After 2 h of preincubation of 9aa (=100 μg/mL) with P22 in the dark, inactivations were carried out at varying light intensities. A plot of log k_{obsd} vs. log (light intensity) gave a straight line with a slope of 0.86 (data not shown). Thus, the inactivation rate depends on the 0.86 power of the light intensity; this value is close to 1 and indicates a monophotonic process.

Discussion

The DNA within a phage capsid is close-packed with a hydrated density of 1.25 g/cm^3 and a center to center spacing between strands of 24 Å (Earnshaw & Casjens, 1980). The strands are ordered, probably as concentric coils (Earnshaw et al., 1979). We have been particularly interested in determining, for this biologically relevant state of DNA, the nature of the acridine/DNA complex which provides the target for photoinactivation.

The 9aa/DNA binding complex, crucial for inactivation, could have 9aa bound to the DNA in either the intercalated or the backbone mode, or both. To determine which case is more likely, initially, we will consider the equilibrium binding and inactivation data (Figure 1) and then the kinetic binding and inactivation data (Figures 2–5).

The binding curve that we observed in Figure 1 (closed circles) bears a resemblance to those observed for the binding of various acridines to DNA free in solution (Peacocke, 1973; Porumb, 1978). Two binding modes are commonly observed, process I and process II, which correspond to acridine intercalation between the DNA base pairs and as subsequent binding of additional acridine molecules to the phosphates along the DNA backbone, respectively. Intercalation results in tighter binding (process I) (Li & Crothers, 1969; Sakore et al., 1977; Tsai et al., 1977; Jain et al., 1977; Sobell et al., 1977; Neidle et al., 1977; Young & Kallenback, 1980), and the dyes often show what appears to be negative cooperativity in binding (Crothers, 1968; Li & Crothers, 1968; Armstrong et al., 1970; Bauer & Vinograd, 1970; Dourlent & Hogrel, 1976). Backbone binding is weaker (process II), and positive cooperativity has been observed in the case of dye binding to DNA and other polyanions, (Weill & Calvin, 1963; Schwarz, 1970; Schwartz & Klose, 1972; Peacocke, 1973; Dourlent & Hogrel, 1976; Yamaoka & Masujima, 1978). Positive cooperativity has been attributed to the face to face stacking of acridines along the DNA backbone.

The most reasonable interpretation of the binding data in Figure 1 is that we are also observing two binding modes: process I (intercalation) at lower [9aa] and process II (backbone binding) at higher [9aa]. The second binding mode at higher [9aa] is likely to result from backbone binding (process II) because it is weaker, and because it shows apparent positive cooperativity. We are less certain about the identity of the binding mode at lower [9aa] because of its smaller magnitude, but the most reasonable interpretation of these data is that they indicate tighter, intercalative binding (i.e., process

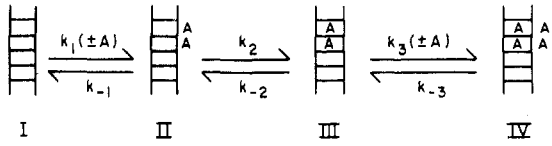

	k_1	k_2	k_3
Model 1	1.3 min^{-1}	> k_1	0.11 min^{-1}
Model 2	1.3 min^{-1}	0.11 min^{-1}	> k_2

FIGURE 6: Models for the kinetics of binding of 9aa and P22 DNA. In both models, backbone binding by 9aa is represented with an A on the outside of a ladder (species II and IV). Intercalative binding is depicted with an A between the rungs of the ladder (species III and IV). The values for the rate constants are taken from Figure 2 with [9aa] = 100 μg/mL.

I). In the case of dye binding to the DNA of other viruses, similar binding curves have been observed (Carlberg-Bacq, 1977a).

The smooth curve drawn through the rate constants for inactivation (open circles, Figure 1) approximately follows the process II phase of the binding curve, and both show a steep dependence on [9aa] below saturation. At lower [9aa], when only process I is observed in the binding curve, the inactivation rate constants are virtually equal to zero. The similarities between the process II binding curve and the curve for the rate constants of inactivation suggest that the two phenomena are related, i.e., that inactivation is associated with 9aa binding to the DNA backbone. (One possible explanation for why the inactivation and binding curves are not perfectly coincident is discussed below.)

Kinetic Models for the 9aa Binding Reaction. Two kinetic binding steps were observed in Figure 2; an initial, rapid step leading to the formation of species X (Scheme I) and a second, slower step leading to the formation of species Y (Scheme I). Figure 6 shows two models which are consistent with all of our kinetic binding data. Both models involve four species of DNA/9aa complexes; species I, no 9aa; species II, 9aa bound only to the backbone; species III, 9aa intercalated; species IV, 9aa bound to the backbone of a region that also has intercalated molecules. The essential difference between the models is the nature of the rapid binding step. According to model 1, the rapid binding step results in the formation of species III (intercalated 9aa), because the second step (k_2) occurs *rapidly* compared to the first step (k_1). In contrast, according to model 2 the rapid binding step results in the formation of species II (backbone-bound 9aa) because the second step (k_2) occurs *slowly* compared to the first step (k_1). In both models, the slow binding step results in the formation of species IV. [We note that model 1 could be modified such that the k_2 step would be rate determining (i.e., with $k_1 > k_2$), if k_1/k_{-1} were small. This leads to the same conclusions. As discussed later in the text, we do not favor this formulation.]

Three arguments can be made which suggest that model 1 is more likely to be correct.

(1) Two observations suggest that the initial, faster phase of the kinetic binding reaction (insert, Figure 2) is associated with the stronger (process I binding of 9aa to P22 observed in Figure 1 while the second, slower phase of the kinetic binding reaction is associated with weaker (process II) binding. First, the second, slower phase only appears at higher [9aa], and its magnitude in OD units corresponded to the magnitude of the weaker binding observed in Figure 1 at higher [9aa] (data not shown). Second, positive cooperativity is seen in the kinetics of the second, slower phase (Figure 2), as it is with weaker (process II) 9aa binding (Figure 1). These associations suggest that the slower kinetic phase results from the binding of 9aa to the DNA backbone, i.e., that model 1 is correct. Furthermore, the correlation between the kinetics of inactivation and the kinetics of the slower binding step (Figures 4 and 5) also suggests that inactivation results from 9aa binding to the DNA backbone.

(2) Piette et al. (1978a, 1979b) have proposed that the peroxide radical mechanism of photodynamic inactivation is favored when dyes are bound in the intercalative mode. The radical process is believed to be biphotonic, while the singlet oxygen mechanism is monophotonic (Van de Vorst & Lion, 1971, 1973). The inactivation we see is likely to be due to a singlet oxygen, nonintercalative-type mechanism, because it is monophotonic, and it is enhanced in D_2O and is inhibited by sodium azide (Bryant & King, 1985). Thus, our results suggest a nonintercalative mode of inactivation.

(3) According to model 2 of Figure 6, the formation of both the backbone-bound 9aa species (II) and the intercalated species (III) is much slower (approximately 10^5 times) for the phage than for the corresponding reaction with DNA, which is free in solution (Kubota & Motoda, 1980). It is sensible that the formation of the backbone-bound species is much slower, because of the barrier to 9aa diffusion posed by the phage capsid. However, it is unclear why the subsequent rearrangement to give intercalated 9aa molecules would be so much slower in phage compared to DNA free in solution. [McCall and Bloomfield (1976a,b) have discussed reasons why this rearrangement might be slow, due to steric constraints on the DNA within the phage head.] Model 1 does not require a large retardation of the rate of the intercalation reaction.

Recently, Houba-Herin et al. (1982) showed that in contrast to some other dyes, 9aa in solution did not generate singlet oxygen efficiently. These findings are not necessarily inconsistent with our results. In earlier work, we showed that both proflavin and acridine yellow inactivated P22 more rapidly than 9aa (Bryant & King, 1985). These two compounds also were more active than 9aa in singlet oxygen production in solution (Houba-Herin et al., 1982). Thus, 9aa might not produce singlet oxygen at levels sufficiently high to be detectable by the methods employed by these workers, yet be produced at an efficiency sufficient to inactivate P22.

Our results contrast with those for the proflavin-induced and acridine orange induced photodynamic inactivation of T4 and pneumococcal DNA, respectively, where inactivation correlated with dye intercalation (Fujita, 1970; Piette et al., 1978b). However, it has been suggested that thiopyronine inactivation of T4 involves the backbone binding mode. Further work is needed to understand why different, but related, dyes show different inactivation mechanisms in different systems. However, it is possible that dye inactivation from the backbone binding mode involves damage to nearby critical proteins while from the intercalated mode, it involves DNA damage. The dominant mode of inactivation by a dye would depend on the relative sensitivities of the DNA vs. protein targets, the orientation of the dye vis-â-vis these targets, the efficiency of the dye in the generation of the proximate damaging agent, and the ability of the dye to reach and bind to its target.

Implications of 9aa Binding with Condensed DNA. One implication of model 1 is that $k_1 = 10k_3$, although both represent backbone binding reactions. This difference must result from the fact that binding by k_3 occurs to a phage whose DNA is already filled with intercalated acridines. Because phage DNA is confined within the capsid and is tightly packed (Earnshaw & Harrison, 1977), it is expected that backbone

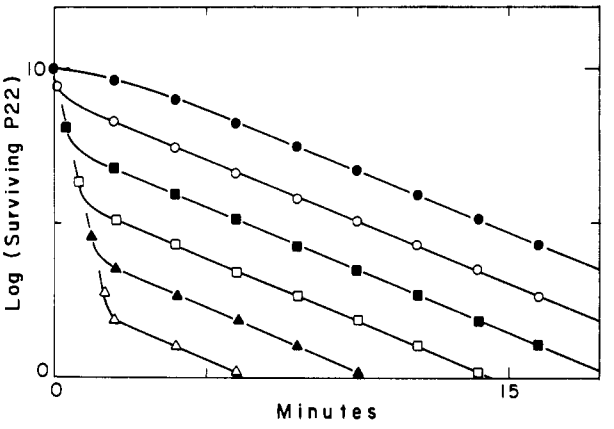

FIGURE 7: Hypothetical inactivation curves calculated by assuming a two-step sequential binding reaction and a *single* 9aa target site within the P22 genome responsible for photoinactivation. These curves were calculated for a hypothetical experiment qualitatively similar to the one presented in Figure 3. The two rate constants associated with 9aa binding to the P22 DNA (analogous to k_X and k_Y in Scheme I) were set at 1.0 min^{-1}. The dark preincubation times were varied: (●) 0 min; (○) 4 min; (■) 8 min; (□) 12 min; (▲) 16 min; (△) 20 min.

binding would be more difficult following the further crowding that results from the intercalated acridines. It is also possible that, following intercalation, the intrinsic stability of the backbone-bound species might be decreased because of conformational changes in the DNA structure.

As enumerated above, the rate constants for 9aa binding to DNA within the P22 particle are different from binding to DNA in solution. In contrast, equilibrium constants are not; the binding constant for 9aa intercalation to P22 particles must be <10 μg/mL (Figure 1), while the constant for 9aa with (calf thymus) DNA is approximately 10 μg/mL (Drummond et al., 1965). Although data for backbone (process II) binding are not available for 9aa, the binding of other acridines to DNA free in solution does not show the "bump" observed in Figure 1 at [9aa] of 50 μg/mL. We can offer no rationale for this effect; however, it must surely reflect the fact that the condensed DNA inside the phage head behaves differently from DNA in solution.

More Than One 9aa Molecule Can Take Part in the Activation Process. Previous work from this laboratory has indicated that the crucial targets for macromolecular damage leading to inactivation are several P22 particle proteins, gp7, gp16 and gp20, which are known to be involved in the DNA injection process (Bryant & King, 1985). It is likely that 9aa must be bound near these proteins before inactivation can occur and that the entire target complex includes these proteins as well as the nearby, crucial 9aa binding site(s). The close correlation between the behavior of the inactivation processes and the binding processes (Figures 1, 4, and 5) suggests that the 9aa binding sites crucial for inactivation behave similarly to the bulk of the 9aa binding sites. However, the correlations are not exact, and this suggests that the inactivation experiments are differentially probing phenomena in a specific local environment within the phage particle.

Our data allow us to evaluate (to a limited extent) the size of the 9aa binding site(s) within the target complex. The results in Figure 4 demonstrate that the rate of the inactivation reaction is directly proportional to the amount of 9aa bound to the backbone of the P22 DNA. This implies that there must be more than one crucial 9aa binding site in the P22 genome which is responsible for inactivation. If there were a single site, then those phage whose crucial site was filled would be inactivated at one rate, while those whose site was unfilled

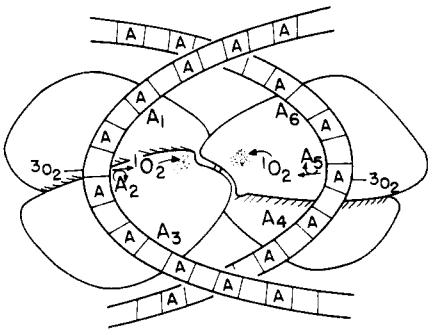

FIGURE 8: Models of the arrangement of the crucial target for the inactivation by P22 by DNA. 9aa molecules bound to the DNA backbone in the vicinity of one or more of the DNA injection proteins (gp7, gp16, and gp20) are shown to be able to damage these protein targets via the production of singlet oxygen. The target could be a single, particularly sensitive (or critical) protein, or any of a number of these proteins, where damage to one results in P22 inviability.

would be inactivated by a slower rate associated with the filling of that site. Phage inactivation by a model with *only one* crucial 9aa binding site, two kinetically significant binding steps, and an inactivation step would give hypothetical results like those in Figure 7. In Figure 7, with increasing preincubation in the dark, only the *fraction* of phage being inactivated by the two rates changes; i.e., the *fraction* of phage killed at the faster rate increases as a function of preincubation time in the dark. Continuously varying initial rates of inactivation are not predicted, which contrasts with the actual data shown in Figure 3. These data indicate that there must be multiple 9aa target sites within a P22 particle, such that, as more sites become filled, the crucial inactivating event becomes more probable. (For example, a phage having only 2 of its 10 binding sites filled would be 20% as likely to be inactivated as one with all 10 sites filled.) Our data do not permit an accurate evaluation of the number of crucial sites, but it is clearly more than five. A complete mathematical treatment of the inactivation data in Figure 3 as well as data that show more 9aa binds to P22 in the dark than in the light (an unexpected finding) will be presented elsewhere.

Figure 8 shows how multiple binding sites might be arranged. Several 9aa molecules are depicted as being positioned such that they can damage a crucial site on one (or more) critical P22 particle protein(s). Phage particles contain 10–20 copies of these DNA-injection proteins (King et al., 1976). Inactivation could result from damage to any one of these proteins or, selectively, to one in particular.

CONCLUSIONS

Several major conclusions were drawn from the work reported above. (1) Two kinetically distinguishable steps in the binding of 9aa to P22 were discernible: a rapid step resulting in 9aa intercalation and a slower step resulting in the binding of additional 9aa to the DNA backbone. (2) Photodynamic inactivation of P22 was shown to correlate with the binding of 9aa to the DNA backbone, which implies that this species is involved in the photoexcitation leading to the formation of the inactivating agent, singlet oxygen. (3) The data support a model in which more than one 9aa molecule can give rise to inactivating events, and as the number of 9aa molecules bound in crucial sites in P22 DNA increases, the probability of P22 inactivation increases proportionally.

ACKNOWLEDGMENTS

We thank Jennice Phillips for careful preparation of the manuscript.

Registry No. 9-Aminoacridine, 90-45-9.

REFERENCES

Adams, M. (1959) *Bacteriophages*, Interscience Publishers, New York.

Alberts, A. (1966) *The Acridines*, Willian Clowes and Sons, Ltd., London.

Armstrong, R. W., Kurucsev, T., & Strauss, U. P. (1970) *J. Am. Chem. Soc. 92*, 3174–3181.

Bauer, W., & Vinograd, J. (1970) *J. Mol. Biol. 47*, 419–435.

Blake, A., & Peacock, A. R. (1968) *Biopolymers 6*, 1225–1253.

Botstein, D., Waddell, C. H., & King, J. (1973) *J. Mol. Biol. 80*, 669–695.

Bryant, J., & King, J. (1985) *J. Mol. Biol. 180*, 837–863.

Calberg-Bacq, C. M., Siquet-Descans, F., Peitte, J., & Van de Vorst, A. (1977a) *Biochim. Biophys. Acta 477*, 239–249.

Calberg-Bacq, C. M., Siquet-Descans, F., Peitte, J., & Van de Vorst, A. (1977b) *Photochem. Photobiol. 26*, 573–579.

Crothers, D. M. (1968) *Biopolymers 6*, 575–584.

Dourlent, M., & Hogrel, J. F. (1976) *Biopolymers 15*, 29–41.

Drummond, D. S., Simpson-Gildemeister, V. F. W., & Peacocke, A. R. (1965) *Biopolymers 3*, 135–153.

Earnshaw, W. C., & Harrison, S. C. (1977) *Nature (London) 268*, 598–602.

Earnshaw, W. C., & King, J. (1978) *J. Mol. Biol. 126*, 721–747.

Earnshaw, W. C., Casjens, S., & Harrison, S. C. (1976) *J. Mol. Biol. 104*, 387–410.

Foote, C. S. (1968) *Science (Washington, D.C.) 162*, 963–970.

Fujita, J. (1970) *J. Sci. Hiroshima Univ. Sor. A-2 4*, 195.

Jain, S. C., Tsai, C., & Sobell, H. M. (1977) *J. Mol. Biol. 114*, 317–331.

King, J., Bottstein, D., Casjens, S., Earnshaw, W., Harrison, S. C., & Lenk, E. V. (1976) *Philos. Trans. R. Soc. London, B, 276*, 7–49.

Kobayashi, K., & Ito, T. (1977) *Photochem. Photobiol. 25*, 385–388.

Kubota, Y., & Motoda, Y. (1980) *Biochemistry 19*, 418–419.

Lerman, L. S. (1961) *J. Mol. Biol. 3*, 18–30.

Lerman, L. S. (1963) *Proc. Natl. Acad. Sci. U.S.A. 49*, 94–102.

Li, H. J., & Crothers, D. (1969) *J. Mol. Biol. 39*, 461–477.

Lochman, E. R., & Micheler, A. (1973) *Physicochemical Properties of Nucleic Acids* (Duchesne, J., Ed.) Vol. 1, pp 223–267, Academic Press, New York.

Loechler, E. L., & Hollocher, T. C. (1980) *J. Am. Chem. Soc. 102*, 7312–7321.

McCall, P. J., & Bloomfield, V. A. (1976) *Biopolymers 15*, 2323–2336.

McLaren, A. D., & Shugar, D. (1964) *Photochemistry of Proteins and Nucleic Acids*, pp 313–319, Paragon Press, New York.

Murialdo, H., & Becker, A. (1978) *Microbiol. Rev. 42*, 529–576.

Neidle, S., Achari, A., Taylor, G. L., Berman, H. M., Carrell, H. L., Glusker, J. D., & Stallings, W. C. (1977) *Nature (London) 269*, 304–307.

Norden, B., & Tjerneld, F. (1982) *Biopolymers 21*, 1713–1734.

Peacocke, A. R. (1973) *Chem. Heterocycl. Compd. 9*, 723–757.

Piette, J., Calberg-Bacq, C. M., & Van de Vorst, A. (1977) *Photochem. Photobiol. 26*, 377–382.

Piette, J., Calberg-Bacq, C. M., & Van de Vorst, A. (1978a) *Int. J. Radiat. Biol. Relat. Stud. Phys., Chem. Med. 34*, 213–221.

Piette, J., Calberg-Bacq, C. M., Cannistrato, S., & Van de Vorst, A. (1978b) *Int. J. Radiat. Biol. Relat. Stud. Phys., Chem. Med. 34*, 223–232.

Piette, J., Lopez, M., Calberg-Bacq, C. M., & Van de Vorst, A. (1981a) *Int. J. Radiat. Biol. Relat. Stud. Phys., Chem. Med. 40*, 421–433.

Piette, J., Calberg-Bacq, C. M., & Van de Vorst, A. (1981b) *Photochem. Photobiol. 33*, 325–333.

Porumb, H. (1978) *Prog. Biophys. Mol. Biol. 34*, 175–195.

Sakore, T. D., Jain, S. C., Tsai, C., & Sobell, H. M. (1977) *Proc. Natl. Acad. Sci. U.S.A. 74*, 188–192.

Schwartz, G. (1970) *Eur. J. Biochem. 12*, 442–453.

Schwartz, G., & Klose, S. (1972) *Eur. J. Biochem. 29*, 249–256.

Sharp, P. A., & Bloomfield, V. A. (1970) *Biochem. Biophys. Res. Commun. 39*, 407–413.

Sobell, H. M., Tsai, C., Jain, S. C., & Gilbert, S. G. (1977) *J. Mol. Biol. 114*, 333–365.

Spikes, J. D. (1977) in *The Science of Photobiology* (Smith, K. C., Ed.) pp 87–112, Plenum Press, New York.

Susskind, N., Botstein, D., & Wright, A. (1974) *Virology 62*, 350–366.

Tsai, C., Jain, S. C., & Sobell, H. M. (1977) *J. Mol. Biol. 114*, 301–315.

Van de Vorst, A., & Lion, Y. (1971) *Biochim. Biophys. Acta 246*, 421–429.

Van de Vorst, A., & Lion, Y. (1973) *Biochim. Biophys. Acta 294*, 349–355.

Weill, G., & Calvin, M. (1963) *Biopolymers 1*, 401–417.

Welsh, J. N., & Adams, M. H. (1954) *J. Bacteriol. 68*, 122–127.

Yamamoto, N. (1958) *J. Bacteriol. 75*, 443–448.

Yamaoka, K., & Masujima, M. (1978) *Biopolymers 17*, 2485–2501.

Young, P. R., & Kallenbach, N. R. (1980) *Proc. Natl. Acad. Sci. U.S.A. 49*, 6453–6457.

Young, P. R., & Kallenbach, N. R. (1981) *J. Mol. Biol. 145*, 785–813.